# Design of a Bearingless Segment Motor *

Wolfgang Gruber and Wolfgang Amrhein
*Institute of Electrical Drives and Power Electronics*
*Johannes Kepler University Linz*
*Altenbergerstr. 69, 4040 Linz, Austria*
*wolfgang.gruber@jku.at*

***Abstract* – Active magnetic bearings and bearingless motors have begun to be used in industry and medical technology. When the rotor is short with respect to its diameter, it is possible to stabilize three degrees of freedom passively by reluctance forces. For this type of motor a new approach to a mechanical design is presented – the Bearingless Segment Motor.**

**This paper deduces a model of the new motor for current injection. Finite element simulations allow the optimisation of force and torque, the reduction of cogging torque and reluctance forces as well as the consideration of the passive radial and passive axial stiffness. However, the force distribution and the mathematical model are nonlinear. Therefore a suitable nonlinear control scheme is presented. The introduction of a prototype and first measurements complete the paper.**

***Index Terms* – bearingless segment motor, bearingless drive, force and torque calculation, nonlinear control scheme**

## I. Introduction

During the last few years a lot of research work has been done to work out different concepts for bearingless drives and bearingless motors [1]. First serial products entered the market and it turned out that this kind of technology has a lot of advantages [2], [3]. Bearingless drives have almost unlimited lifetime, no lubrication and it is possible to satisfy high demands on cleanliness, chemical resistance and tightness. However, for high volume products commercial aspects become almost as important as technical ones. Therefore the mechanical and electrical complexity has to be reduced.

A bearingless motor featuring a very simple mechanical design is the bearingless slice motor with a permanent magnet excited disk-shaped rotor [4]. An advantage of this drive configuration is that the axial position and tilting effects are passively stabilized by reluctance forces and only three degrees of freedom have to be controlled actively [5]. However, this motor principle can only be applied if the demands on stiffness in axial and tilting direction are not too strict. A further mechanical simplification can be achieved by employing concentrated instead of distributed coils [6], [7]. Moreover it is possible to reduce the complexity of the inverter topology by connecting all phase currents in star.

For this type of bearingless motors a new approach to a mechanical design is presented, which minimizes the volume of the ferromagnetic stator material. This leads to a cost effective stator design and furthermore to a significant reduction of weight, especially for large-scale systems.

### A. *Bearingless Segment Motor*

The Bearingless Segment Motor is characterized by four or more separate stator segments, where each contributes to generate radial levitation forces and motor torque. Fig. 1 shows a constructional example of the proposed design.

Unlike classical electromagnetic radial bearings, which show a similar design, the windings of the stator segments are electrically fed with different current components. By this means the number of actively controlled degrees of freedom is extended by the motor torque. Although the mechanical setup becomes simple, there is a high grade of harmonics in the magnetomotive force and in the flux distribution. This leads to a nonlinear characteristic of force and torque generation as well as disturbing effects like cogging torque, radial reluctance forces and torque ripples. Due to the high number of permanent magnet rotor poles, which is characteristic for the basic concept, the cross sections of ferromagnetic flux paths become very small.

Possible fields of applications for the Bearingless Segment Motor are pumps, fans or blowers with special requirements on lifetime, tightness, cleanliness, weight or smooth running.

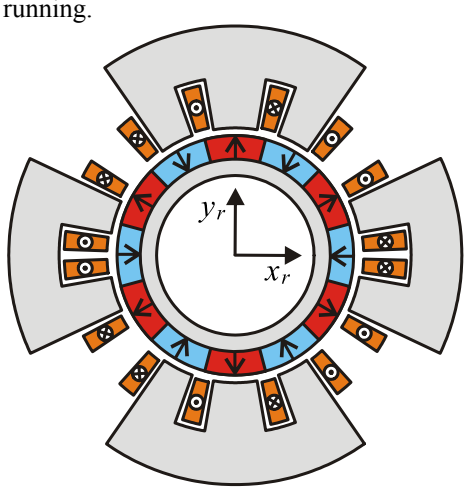


Fig. 1: Bearingless Segment Motor with four stator elements, where segments with two and three pole shoes are used

* This research project was kindly supported by the Austrian Science Fund (FWF) under contract P17523-N07. The authors thank the Austrian Government for the support.

## II. Mathematical Model

### A. Force and Torque Calculation

A mathematical description of force and torque generation of the Bearingless Segment Motor can be given based on the Fourier coefficients of the electromagnetic field variables. Using the Maxwell Stress Tensor the radial forces and the electromagnetic torque may be formulated as

$$\begin{pmatrix} F_x \\ F_y \\ M_z \end{pmatrix} = \begin{pmatrix} \mathbf{i_S}^T & \mathbf{0} & \mathbf{0} \\ \mathbf{0} & \mathbf{i_S}^T & \mathbf{0} \\ \mathbf{0} & \mathbf{0} & \mathbf{i_S}^T \end{pmatrix} \begin{pmatrix} \mathbf{M_{Q,x}}(\mathbf{x_r},\varphi) \\ \mathbf{M_{Q,y}}(\mathbf{x_r},\varphi) \\ \mathbf{N_{Q,z}}(\mathbf{x_r},\varphi) \end{pmatrix} \mathbf{i_S} + \begin{pmatrix} \mathbf{M_{L,x}}(\mathbf{x_r},\varphi) \\ \mathbf{M_{L,y}}(\mathbf{x_r},\varphi) \\ \mathbf{N_{L,z}}(\mathbf{x_r},\varphi) \end{pmatrix} \mathbf{i_S} + \begin{pmatrix} \mathbf{M_{C,x}}(\mathbf{x_r},\varphi) \\ \mathbf{M_{C,y}}(\mathbf{x_r},\varphi) \\ \mathbf{N_{C,z}}(\mathbf{x_r},\varphi) \end{pmatrix}, \quad (1)$$

with the current vector $\mathbf{i_S}$, the rotor displacement vector $\mathbf{x_r}=[x_r, y_r]^T$ and the rotor angle $\varphi$ [8].

Simplifications of this equation can be achieved due to surface mounted permanent magnets on the rotor, which lead to small elements in the matrices $\mathbf{M_{Q,x}}$, $\mathbf{M_{Q,y}}$ and $\mathbf{N_{Q,z}}$. Assuming a stable operation point of the rotor in the centered position ($\mathbf{x}=\mathbf{0}$) the matrices can be linearized via Taylor series approximation around $\mathbf{i_S}=\mathbf{0}$ to

$$\begin{aligned} \begin{pmatrix} F_x \\ F_y \\ M_z \end{pmatrix} &\approx \begin{pmatrix} \mathbf{M_{L,x}}(\mathbf{0},\varphi) \\ \mathbf{M_{L,y}}(\mathbf{0},\varphi) \\ \mathbf{N_{L,z}}(\mathbf{0},\varphi) \end{pmatrix} \mathbf{i_S} + \begin{pmatrix} \mathbf{M_{C,x}}(\mathbf{0},\varphi) \\ \mathbf{M_{C,y}}(\mathbf{0},\varphi) \\ \mathbf{N_{C,z}}(\mathbf{0},\varphi) \end{pmatrix} + \\ &+ \begin{pmatrix} k_{xx}(\mathbf{0},\varphi) & k_{xy}(\mathbf{0},\varphi) \\ k_{yx}(\mathbf{0},\varphi) & k_{yy}(\mathbf{0},\varphi) \end{pmatrix} \mathbf{x_r} \\ &\approx \mathbf{T_m}(\varphi)\mathbf{i_S} + \mathbf{T_c}(\varphi) + \mathbf{K_x}(\varphi)\mathbf{x_r}. \end{aligned} \quad (2)$$

As a result the bearing forces and the motor torque are only nonlinear functions of the rotor angle.

### B. Overall Model for Current Injection

To deduce the complete model of the bearingless motor, the mechanical equations of motion

$$\begin{pmatrix} m & 0 & 0 \\ 0 & m & 0 \\ 0 & 0 & J_z \end{pmatrix} \begin{pmatrix} \ddot{x}_r \\ \ddot{y}_r \\ \ddot{\varphi} \end{pmatrix} = \mathbf{M} \begin{pmatrix} \ddot{x}_r \\ \ddot{y}_r \\ \ddot{\varphi} \end{pmatrix} = \begin{pmatrix} F_x \\ F_y \\ M_z \end{pmatrix} \quad (3)$$

must be taken into account, where $m$ denotes the mass and $J_z$ the inertia of the rotor. $\mathbf{M}$ represents the mass matrix. Combining (2) and (3), the model of the bearingless motor can be derived as a system of nonlinear first order differential equations as follows[†]

$$\dot{\mathbf{x}} = \begin{pmatrix} \mathbf{O}_{3\times3} & \mathbf{E}_3 \\ \mathbf{M}^{-1}\mathbf{K_x}(\varphi) & \mathbf{O}_{3\times3} \end{pmatrix} \mathbf{x} + \begin{pmatrix} \mathbf{O}_{3\times m} \\ \mathbf{M}^{-1}\mathbf{T_m}(\varphi) \end{pmatrix} \mathbf{i_S} + \begin{pmatrix} \mathbf{O}_{3\times1} \\ \mathbf{M}^{-1}\mathbf{T_c}(\varphi) \end{pmatrix}, \quad (4)$$

with $\mathbf{i_s}$ as the actuating variable. The state vector $\mathbf{x}$ is defined as

$$\mathbf{x} = \begin{pmatrix} x_r & y_r & \varphi & \dot{x}_r & \dot{y}_r & \dot{\varphi} \end{pmatrix}^T. \quad (5)$$

## III. Finite Element Simulations

### A. Stator and Rotor Design

The mechanical design of the proposed Bearingless Segment Motor focuses on systems with four equal stator elements in symmetric arrangement. It turned out from finite element simulations that stator elements with three pole shoes show a better performance than two pole shoe segments. This assessment holds true for bearing forces and motor torque comparing stator elements of the same angular size and coils with equal ampere-turns. Fig. 2 shows the design drawing of one of the four equal chosen stator segments.

Using four stator elements often leads to the fact that the cogging torque is quite high compared to the producible torque of the motor. This arises from the fact that the cogging torque sums up of the sole segment cogging torques, due to the even-numbered rotor poles. Furthermore the cogging torque is proportional to the derivate of the magnetic flux density with respect to the rotor angle, making bended magnet segments of constant height in the rotor a bad choice. In this respect circular magnet segments, illustrated in Fig. 3, show a far better behavior.

To ensure enough space for the position and angular sensors between the stator segments the amount of pole pairs in the rotor was set to six. The rotor consists of bonded NdFeB magnets with a magnetic remanence of 0.7 *T*. That is why the airgap between rotor and stator has to be small to get the necessary flux essential for practical force and torque generation.

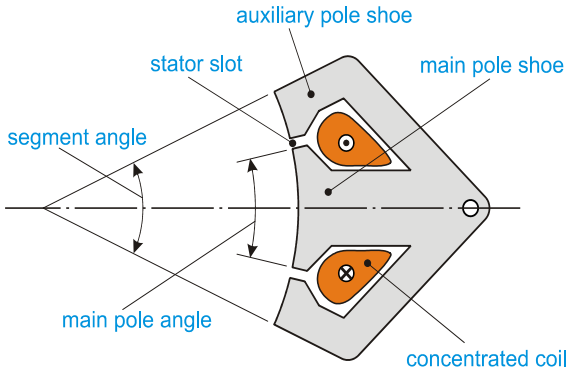


Fig. 2: Stator segment

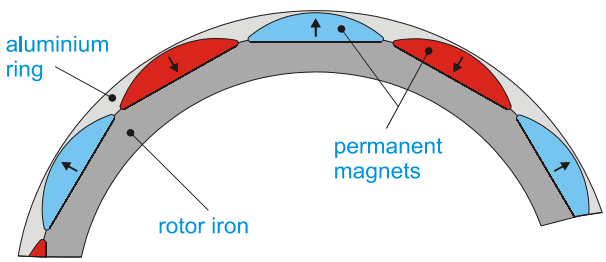


Fig. 3: Rotor design

[†] $\mathbf{O}_{n\times m}$ represents a zero matrix of the dimension $n \times m$ and $\mathbf{E}_n$ stands for an identity matrix of the dimension $n$.

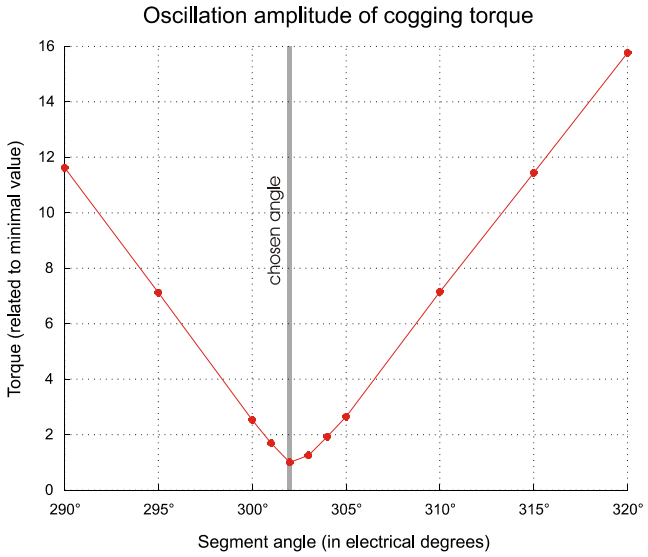


Fig. 4: Optimization of the cogging torque by changing the stator segment angle

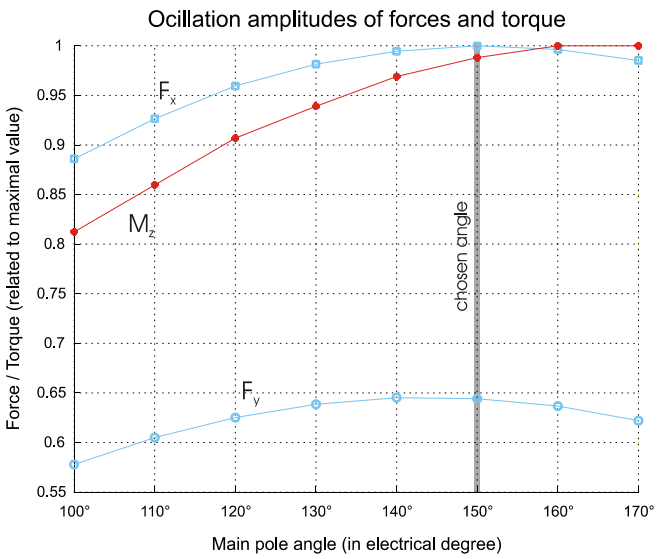


Fig. 5: Optimization of the bearing forces by parameter variation of the main pole angle

### *B. Parameter Variation*

2D finite element simulations were used to minimize the cogging torque and optimize the bearing forces. The varied parameters are the stator segment angle and the main pole angle. A constant stator slot of 2 *mm* was maintained over all simulations to allow the use of a needle winding system to manufacture the concentrated windings.

Fig. 4 shows the result of the segment angle variation to reduce cogging torque. In this series the main pole angle remained constant at 180° and the coils were not energized. Compared to a variation of the segment angle there is nearly no influence in the cogging torque when the main pole angle is diversified. Reluctance forces are naturally negligible for symmetric four stator element designs. Choosing a segment angle of 302° the cogging torque as well as the reluctance forces can be neglected in centered rotor position. This fact leads to small entries in the matrix $\mathbf{T_c}(\varphi)$, allowing to set $\mathbf{T_c}(\varphi)\approx\mathbf{0}$.

To increase the bearing forces by variation of the stator main pole angle was the next step of the optimization of the stator geometry. The force and torque characteristics of the design were simulated with only one coil supplied with constant current. Fig. 5 gives the evaluation of the simulation series, which leads to an optimum main pole angle of 150° with regard to maximum bearing forces.

The 2D finite element simulations were controlled to some extent with 3D simulations, which showed excellent correlation. In case of the Bearingless Segment Motor it is practicable to calculate the matrix $\mathbf{T_m}(\varphi)$ from the force and torque characteristics created by just one coil with the aid of rotary matrices, because the stator segments do not interfere with each other. Further 3D simulations showed a linear axial and radial stiffness almost independent from the rotor angle $\varphi$. This assertion also holds true for tilting in any direction. Because of that result, it is possible to replace the generally nonlinear matrix $\mathbf{K_x}(\varphi)$ by a constant matrix $\mathbf{K_x}$ as a first approximation.

## IV. Control Algorithm

### *A. Force-Current Matrix $K_m$*

For closed loop operation of a bearingless slice motor the decoupling matrix $\mathbf{K_m}(\varphi)$ [9] has to be found, holding the relation

$$\mathbf{i_S} = \mathbf{K_m}(\varphi)\begin{pmatrix} F_x \\ F_y \\ M_z \end{pmatrix}. \qquad (6)$$

For $\mathbf{i_s}$ having the dimension three, the solution

$$\mathbf{K_m}(\varphi) = \mathbf{T_m}(\varphi)^{-1} \qquad (7)$$

is obvious. To calculate the decoupling matrix at higher dimensions of $\mathbf{i_s}$ additional constraints have to be imposed. A common approach is to minimize the copper losses of the coils by introducing the constraint

$$\mathbf{i_S}^{\mathrm{T}}\,\mathbf{i_S} \rightarrow \min. \qquad (8)$$

Possible matrices satisfying (6) and (8) are given by

$$\mathbf{K_m}(\varphi) = \mathbf{T_m}(\varphi)^T\left(\mathbf{T_m}(\varphi)\mathbf{T_m}(\varphi)^T\right)^{-1}. \qquad (9)$$

For an operation, where the motor phases are connected in star the solution leads to

$$\mathbf{K_m}(\varphi) = \left(\mathbf{T_m}(\varphi)^T - \tfrac{1}{4}\mathbf{I}\,\mathbf{I}^T\mathbf{T_m}(\varphi)^T\right) \cdot\left(\mathbf{T_m}(\varphi)\left(\mathbf{T_m}(\varphi)^T - \tfrac{1}{4}\mathbf{I}\,\mathbf{I}^T\mathbf{T_m}(\varphi)^T\right)\right)^{-1}, \qquad (10)$$

with

$$\mathbf{I} = \begin{bmatrix}1 & 1 & 1 & 1\end{bmatrix}^T. \qquad (11)$$

The verification of the equation

$$\mathbf{T_m}(\varphi)\mathbf{K_m}(\varphi) = \mathbf{E}_n \qquad (12)$$

is possible in any of the calculation rules above.

### B. *Decoupling of Force/Torque Relationship*

In general the current-force-matrix $\mathbf{T_m}(\varphi)$ is fully occupied, meaning that any single current in the coils generates both, forces and torque. Under the condition of a symmetric stator design it becomes possible to decouple the force and torque generation by the multiplication of a constant transition matrix $\mathbf{V}$ [10]. Having a rotor with even pole pairs a suitable decoupling matrix is given by

$$\mathbf{V} = \begin{pmatrix} \mathbf{E}_n & \mathbf{E}_n \\ -\mathbf{E}_n & \mathbf{E}_n \end{pmatrix}. \tag{13}$$

The relations

$$\mathbf{i_s} = \mathbf{V}\,\bar{\mathbf{i}}_\mathbf{s} \tag{14}$$

and

$$\bar{\mathbf{T}}_\mathbf{m}(\varphi) = \mathbf{T_m}(\varphi)\mathbf{V} = \begin{pmatrix} \mathbf{m}(\varphi) & \mathbf{0}\mathbf{0}^T \\ \mathbf{0}^T & \mathbf{n}(\varphi) \end{pmatrix} \tag{15}$$

hold true. The new matrix $\bar{\mathbf{T}}_\mathbf{m}(\varphi)$ has zero values in some of the entries. This also has the effect that there are zero entries in the matrix $\bar{\mathbf{K}}_\mathbf{m}(\varphi)$, obtained when using (9) or (10) with $\bar{\mathbf{T}}_\mathbf{m}(\varphi)$ instead of $\mathbf{T_m}(\varphi)$. That fact yields to less complexity when implementing the control scheme on a microprocessor.

### C. *General Control Scheme for Current Injection*

Applying (14) and (15) to (4) it can be shown that the model for current injection of the bearingless motor can be written as

$$\begin{aligned} \dot{\mathbf{x}} = &\left(\mathbf{A_L} + \mathbf{A_{NL}}(\varphi)\right)\mathbf{x} + \mathbf{B_L}\,\bar{\mathbf{T}}_\mathbf{m}(\varphi)\,\bar{\mathbf{i}}_\mathbf{s} \\ &+\mathbf{B_L}\mathbf{C_{NL}}(\varphi). \end{aligned} \tag{16}$$

The subscript L represents constant matrices and the subscript NL characterizes the nonlinear parts. Using a nonlinear transformation for the actuating variable of the form

$$\bar{\mathbf{i}}_\mathbf{s} = \mathbf{r}(\mathbf{x}) + \mathbf{v}(\mathbf{x})\,\mathbf{u}^* \tag{17}$$

it becomes feasible to linearize nonlinear mathematical models [11], [12]. In case of (16) the choice

$$\bar{\mathbf{i}}_\mathbf{s} = \bar{\mathbf{K}}_\mathbf{m}(\varphi)\left[\mathbf{u}^*(t) - \mathbf{A_{NL}}^*(\varphi)\mathbf{x}(t) - \mathbf{C_{NL}}^*(\varphi)\right] \tag{18}$$

leads to a new linear system

$$\dot{\mathbf{x}} = \mathbf{A_L}\mathbf{x} + \mathbf{B_L}\mathbf{u}^*. \tag{19}$$

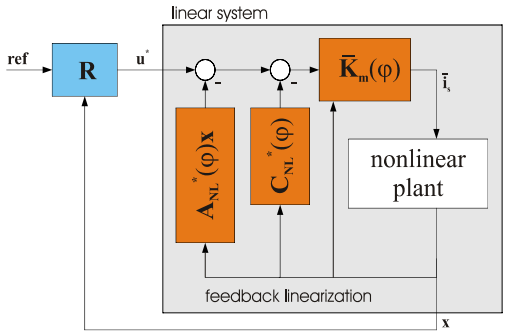


Fig. 6: General control scheme

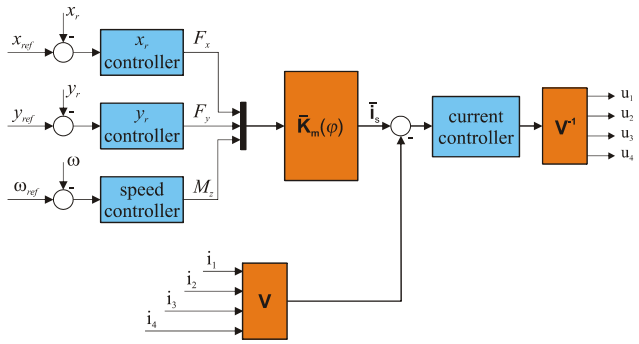


Fig. 7: Implemented control scheme of the proposed bearingless motor

Fig. 6 illustrates the transformation in a block diagram. Taking a closer look, it becomes clear, that the entries of the new actuating vector $\mathbf{u}^*$ might be interpreted as forces in $x_r$ and $y_r$ direction and as torque. It is possible to design position controllers as well as a speed controller using linear time-invariant methods for the overall linear system.

### C. *Control Scheme for the Bearingless Segment Motor*

The control scheme introduced in the previous chapter is valid for any bearingless slice motor. Keeping in mind the introduced Bearingless Segment Motor with four equal stator elements some simplifications appear. First it is possible to neglect the matrix $\mathbf{T_c}(\varphi)$ because of the chosen optimization. Furthermore it was mentioned that the radial stiffness is not dependent on the rotor angle, leading to a constant matrix $\mathbf{K_x}$. This implies that $\mathbf{A_{NL}}(\varphi)$ in (16) and $\mathbf{A_{NL}}^*(\varphi)$ in (18) are zero matrices.

These two preconditions allow a simplification of the control scheme of the discussed Bearingless Segment Motor. The obtained new scheme is presented in Fig. 7. Looking at this block diagram, there is to annotate, that the control scheme is appropriate for a voltage source inverter, making a nested current controller applicable.

## V. Experimental Results

The setup of the designed Bearingless Segment Motor is shown in Fig. 8 and Fig. 9. The axial length to diameter ratio of the rotor is 1 to 10. The force capacity is about 10 *N* and the torque is approximately 0.5 *Nm* at rated current due to the small size of the construction. Simulations show a passive axial stiffness of 4.5 *N/mm*. The tilting stiffness is well over 0.1 *Nm/deg*, even though bonded magnets with a $B_r$ of just 0.7 *T* were used.

Concerning the realization and implementation of the control scheme in hardware, the 16 bit fixed point digital signal processor TMS320F2811 by Texas Instruments is employed. The software is written in ANSI C-code to alleviate modifications or extensions. The controller is capable of a performance up to 150 MIPS, allowing a sampling time of 100 µsec. The controller system is well-integrated in a power electronics which operates with a

Fig. 8: Rotor of the Bearingless Segment Motor prototype

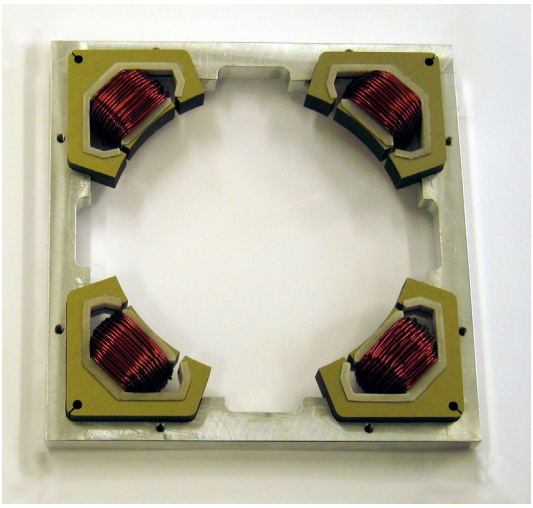

Fig. 9: Stator at assembly

supply voltage of 50 $V$ DC, features five half bridges controlled with a 30 $kHz$ PWM signal and is capable to deliver a maximum power output of 6 $A$ per channel.

To implement the control scheme illustrated in Fig. 7 the four phase currents have to be measured by shunts. Hall respectively eddy current sensors detect the rotor angle and the radial position of the rotor. The angular speed is observed from the rotor angle. The force current matrix $\mathbf{K}_{\mathbf{m}}(\varphi)$ results from (10) and (15) using $\mathbf{T}_{\mathbf{m}}(\varphi)$, which is derived from finite element simulations. The outer position controller for $x_r$ and $y_r$ are standard proportional-integral-derivative (PID) controllers and the speed controller is implemented as proportional-integral (PI) controller. A nested proportional (P) controller is used to increase the electrical dynamics.

To confirm the results obtained by the simulation measurements have been carried out. For this purpose the Bearingless Segment Motor was mounted on a test bed equipped with a cross table to allow measurements of the rotor displacement.

In Fig. 9 the simulated and measured counteracting forces are presented when the rotor is displaced in axial direction.

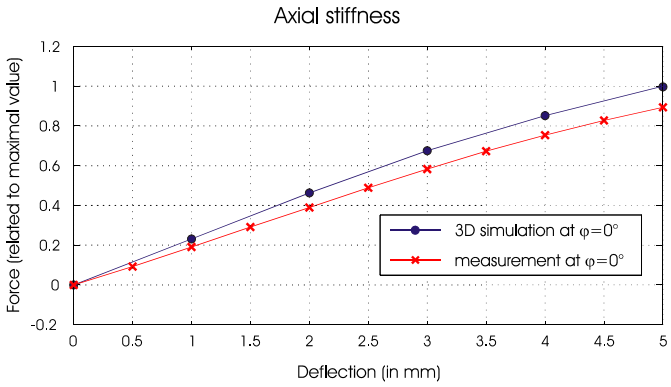


Fig. 9: Counteracting force at axial deflection

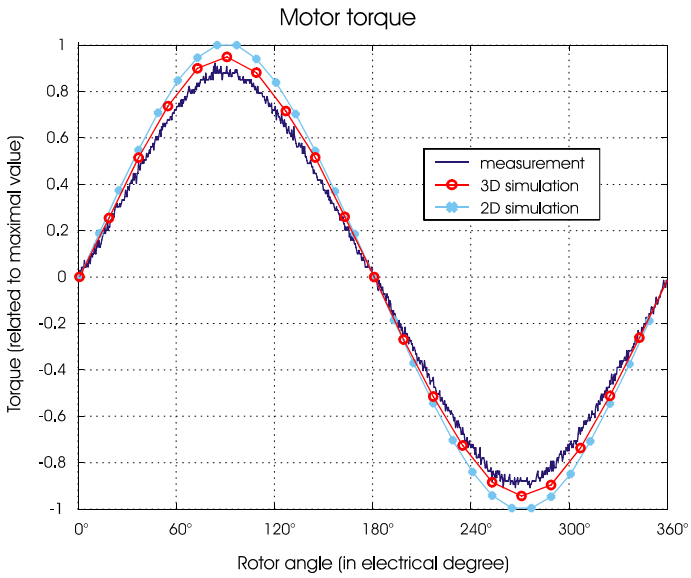


Fig. 10: Simulated and measured torque characteristics

A further measurement of the induced voltage was undertaken to determine the motor torque. From the formula

$$\mathbf{U}_{\mathbf{ind}}{}^{T} = \begin{pmatrix} 0 & 0 & 1 \end{pmatrix} \mathbf{T}_{\mathbf{m}} \Omega \qquad (20)$$

the coherence between the motor torque and the induced voltage becomes clear [13]. In (20) $\Omega$ represents the mechanical speed of the motor.

The difference between measured and simulated results in both presented comparisons Fig. 9 and Fig. 10 is within a range of 10 %.

## CONCLUSION

In this paper a new development of a single phase motor with internal rotor design is introduced. A very simple construction can be achieved using four stator segments with concentrated windings. The nonlinear flux and current distribution leads to a nonlinear force and torque generation. Therefore a special control scheme is required and presented in this paper. Tests with the first prototype show good results in motor and magnetic bearing performance.

## REFERENCES


[1] A. Chiba, T. Fukao, O. Ichikawa, M. Oshima, M. Takemoto, D. G. Dorrell, *"Magnetic Bearings and Bearingless Drives"*, Elsevier, 2005

[2] M. Neff, N. Barletta, R. Schöb, "*Bearingless Centrifugal Pump for Highly Pure Chemicals*", Proc. 8th Int. Symposium on Magnetic Bearings (ISMB8), Mito (Japan), 2002, pp. 283 - 288

[3] S. Ueno, C. Chen, T. Ohishi, K. Matsuada, Y.Okata, Y. Taenaka, T. Masuzawa, "*Design of a Self-Bearing Slice Motor for a Centrifugal Blood Pump*", Proc. Power Conversion Intelligent Motion 1998 (PCIM'98), Nürnberg (Germany), 1998

[4] R. Schöb, N. Barletta, "*Principle and application of a bearingless slice motor*", Proc. 5th Int. Symposium on Magnetic Bearings (ISMB5), Kanazawa (Japan), 1996, p. 313 ff.

[5] K. Nenninger, "*Untersuchungen zum lagerlosen Einphasen-Scheibenläufermotor*", Dissertation, Johannes Kepler Universiy, Linz, 2004

[6] S. Silber, W. Amrhein, "*Design of a Bearingless Single-Phase Motor*", Proc. Power Conversion Intelligent Motion 1998 (PCIM'98), Nürnberg (Germany), 1998, pp. 147-153

[7] W. Amrhein, S. Silber, "*Bearingless Single Phase Motor with Concentrated Full Pitch Windings in Interior Rotor Design*", Proc. 6th Int. Symposium on Magnetic Bearings (ISMB6), Cambridge (United Kingdom), 1998, pp. 476-485

[8] W. Gruber, W. Amrhein, S. Silber, H. Grabner, M. Reisinger, "*Theoretical Analysis of Force and Torque Calculation in Magnetic Bearing Systems with Circular Airgap*", Proc. 8th Int. Symposium on Magnetic Suspension Technology (ISMST8), Dresden (Germany), 2005, pp. 167-171

[9] S. Silber, W. Amrhein, P. Bösch, R. Schöb, B. Barletta, "*Design Aspects of Bearingless Slice Motors*", Proc. 9th Int. Symposium on Magnetic Bearings (ISMB9), Lexington (USA), 2004

[10] H. Grabner, "*Dynamik und Ansteuerkonzepte lagerloser Drehfeld-Scheibenläufermotoren in radialer Bauform*", Dissertation, Johannes Kepler University, 2006

[11] A. Isidori, "*Nonlinear Control Systems*", Springer, 1995

[12] H. Grabner, W. Amrhein, S. Silber, K. Nenninger, "*Nonlinear Feedback Control of a Beraingless Brushless DC Motor*", 6th Int. Conference on Power Electronics and Drive Systems (PEDS2005), Kuala Lumpur (Malaysia), 2005, pp. 366-371

[13] S. Silber, "*Beiträge zum lagerlosen Einphasenmotor*", Dissertation, Johannes Kepler University, 2000